Coordination Chemistry Reviews 255 (2011) 1921–1936

Contents lists available at ScienceDirect

Coordination Chemistry Reviews

journal homepage: www.elsevier.com/locate/ccr

Review

Progress in the study of metal–organic materials applying naphthalene diimide (NDI) ligands

Mei Pan*, Xiao-Ming Lin, Guo-Bi Li, Cheng-Yong Su*

KLGHEI of Environment and Energy Chemistry, MOE Laboratory of Bioinorganic and Synthetic Chemistry, State Key Laboratory of Optoelectronic Materials and Technologies, School of Chemistry and Chemical Engineering, Sun Yat-Sen University, Guangzhou 510275, China

Contents

ARTICLE INFO

Article history:
Received 14 January 2011
Accepted 16 March 2011
Available online 13 April 2011

Keywords:
Naphthalenediimides (NDIs)
Metal–organic materials
Coordination complexes
Analytical techniques
Potential applications

ABSTRACT

1,4,5,8-naphthalenediimide (NDI) derivatives are versatile in coordination and material chemistry due to their large conjugated planar structure and special electron transfer properties. This review presents an overview of metal–organic materials derived from NDIs with their structural models, analytical techniques and potential applications outlined.

1. Introduction

The past few decades have witnessed dramatic progress in the fabrication and self-assembly of metal–organic materials using metal–ligand coordination interactions [1–5]. Their astonishingly diversified spatial and electronic structures determine their versatile properties, functions and applications in such fields as optics, electronics, magnetism, catalysis, sensors and probes, gas storage and separations, host–guest systems, etc. [6–11]. The structures and properties of metal–organic materials are usually synergistically correlated by the judicious combination of metal-based ions/clusters with pre-designed or in situ generated (typically under hydro(solvo)thermal conditions) organic ligands. In partic-

* Corresponding authors. Tel.: +86 20 8411 5178; fax: +86 20 8411 5178.
E-mail addresses: panm@mail.sysu.edu.cn (M. Pan), cesscy@mail.sysu.edu.cn (C.-Y. Su).

0010-8545/$ – see front matter © 2011 Elsevier B.V. All rights reserved.
doi:10.1016/j.ccr.2011.03.013

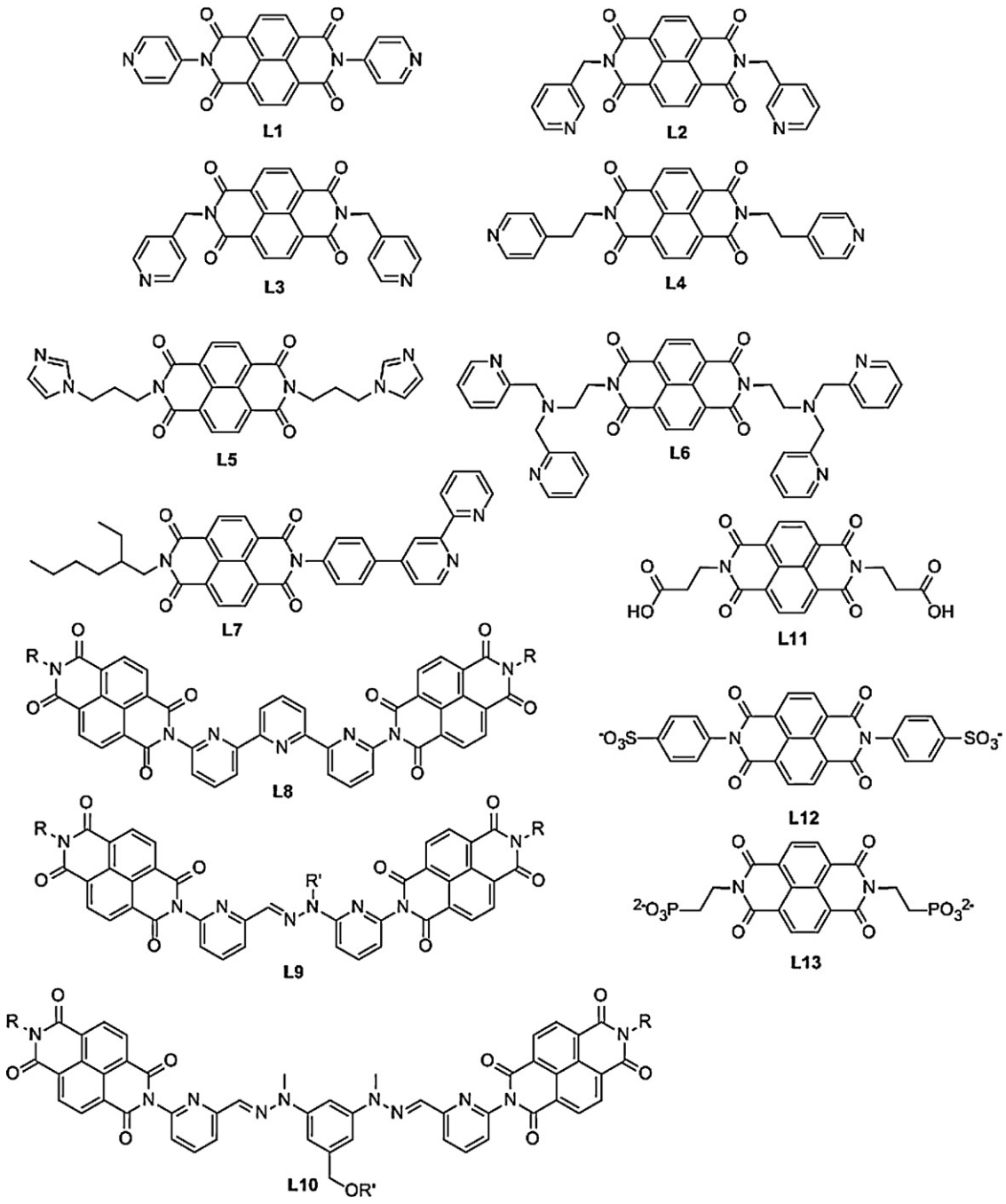

Scheme 1. List of some NDIs ligands mentioned in this article.

ular, the structural diversification of metal–organic materials is greatly dependent upon the functionality and the geometry of the organic ligands used in the assembling process. For instance, numerous ditopic ligands with an "end-core-end" type structural feature have been synthesized to construct a variety of discrete (0D) metal–organic polygons/polyhedra (MOPs), or one-dimensional (1D), two-dimensional (2D) and three-dimensional (3D) metal–organic frameworks (MOFs) [12–17], and in some cases, they are further incorporated into hybrid materials [18–20]. This type of ligand is of interest because they combine two pendant moieties which usually offer conformationally free coordination sites and the central core which generally determines the electronic or spectroscopic character of the coordination complexes.

The central bases selected in most "end-core-end" type organic ligands are aromatic molecules, that are usually introduced to define the conjugate and spectroscopic properties of the ligands. Among these, the 1,4,5,8-naphthalenediimides (NDIs) (also known as naphthalene carbodiimides) have attracted much attention due to their large conjugate planes and special electronic properties. Its coordination complexes show promising applications in such fields as DNA intercalators or luminescent probes [21,22]. Particularly, naphthalenediimides are easily reduced by chemical or electrochemical method ($E = -1.1$ V in CH_2Cl_2 solvent) to form stable radical anions. Therefore, they are widely used as electron acceptor units in artificial photosynthetic systems for solar energy conversion [23–25], or as an electron reservoir in design of catenane and rotaxane supramolecular switches [26,27]. They also show great

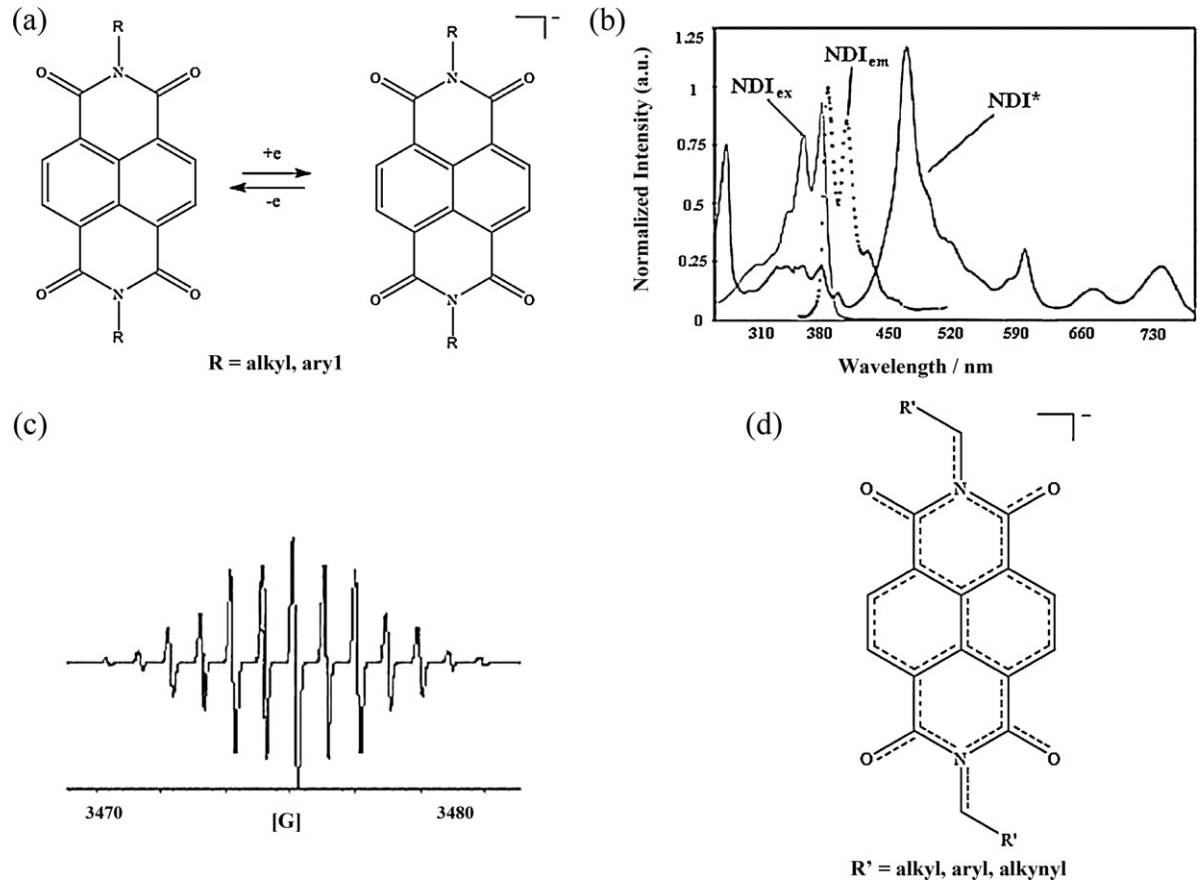

Fig. 1. (a) Bulk electron reduction of NDIs lead to high yields of the corresponding radical anion. (b) Characteristic absorption (thin solid) and emission spectra (dashed, normalised, λ_{ex} = 348 nm) for *N*,*N*′-dipentyl-NDI in DCM are obtained as well as the absorption spectrum for the radical anion of *N*,*N*′-dipentyl-NDI (wide solid) generated by electrochemical reduction. Near-infrared (NIR) absorption bands aid in the unambiguous identification of NDI radical anions. (c) The electron paramagnetic resonance spectrum of the radical anion of *N*,*N*′-dipentyl-NDI in DMF solution shows excellent structure consistent with coupling between the unpaired electron and the naphthalene diimide nitrogen sites and hydrogen atoms and the NCH hydrogen atoms of the appropriate side chains. (d) The radical anion is delocalised over the core naphthalene structure and also extends into hydrocarbon substituents on nitrogen.
Reprinted with permission from Ref. [31]. Copyright 2008 RSC.

tendency to form *n*-type over *p*-type semiconductor materials with high electron mobility [28–30]. The chemistry of naphthalenediimide was excellently summarized by Langford and coworkers in 2008 [31] mainly in organic supramolecular fields. In this article, we will focus on its assemblies, properties and applications in inorganic/metal–organic coordination and hybrid systems with selected references.

2. Basic properties of NDIs

The naphthalenediimides are a class of neutral, planar, and compact aromatic compounds. They are chemically robust while simultaneously electron deficient and redox-active [30]. There are two functionalization sites within this class of compounds, through the diimide nitrogen sites or via core substitution (substitution on the naphthalene core). Different NDI analogues have been designed and applied in both the organic and inorganic/metal–organic supramolecular and material chemistry fields (Scheme 1). Functional groups on the diimide nitrogen sites are usually designed to offer coordination or other linking sites (for example, H-bonds [32,33] or covalent bonds [34–36]), but they can also endow different optical properties to the ligand itself. For example, incorporation of aromatic functional groups will produce non-fluorescent or weakly fluorescent ligands, while introduction of alkyl groups often give rise to the typical white-blue fluorescence. Core substituted NDIs are more efficient in producing highly colorful and functional organic materials with many different photophysical properties. The introduction of weaker π-donors such as alkylamino-, alkoxy-, Cl- or Br-groups accomplishes brilliant colors and intense fluorescence ($\phi \approx 0.5$–0.8). These compounds find potential applications in biomimetic and bioinspired artificial systems [37–41].

The wide application of NDIs also comes from their specific redox-active properties. They undergo chemically or electrochemically single reversible one-electron reduction at moderate potential (NDI: $E^1_{red} = -1.10$ V vs. Fc/Fc^+ in CH_2Cl_2), and stable radical anions will be formed in high yield [42]. The radical anions can be detected by the characteristic and intense visible to near-infrared (NIR) absorption bands, observed at much longer wavelength than the parent NDI ligand (Fig. 1). Therefore, a visible change of initially colorless compound to persistent pink under steady-state or flash irradiation which does not decay over the lifetime of the experiment (100 ms) can support the appearance of NDI^- radical anions under photolysis conditions [28]. Furthermore, EPR affords another tool in determining the existence of NDI^- radical anions. The electronic coupling in this radical system is not confined in the diimide core but extended to the methane ($-CH_2$) carbons on the diimide nitrogen substituents (Fig. 1d) [43]. As a result, NDIs make excellent components for studying electro-induced or photo-induced electron transfer and can be incorporated into larger multi-component assemblies such as field effect transistors (FETs) [28,29], biological mimic models [44], solar energy converters [25] and supramolecular devices and machines [27].

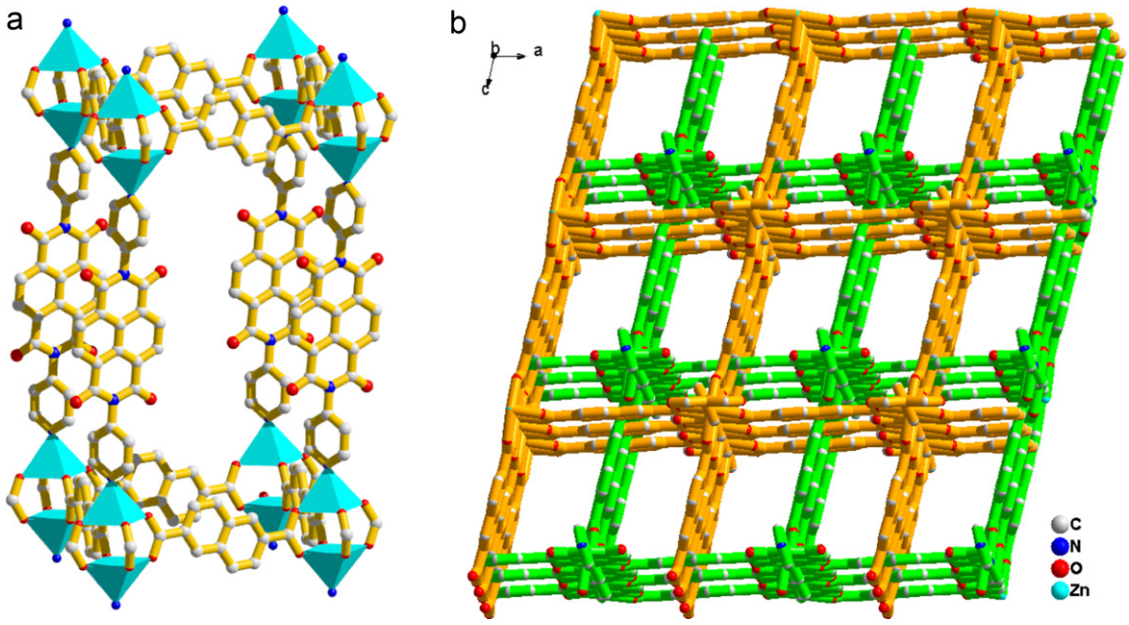

Fig. 2. (a) Crystal structure of complex L1-Zn omitting interwoven second network. (b) Packing diagram of **L1**-Zn showing 2-fold interpenetration [46].

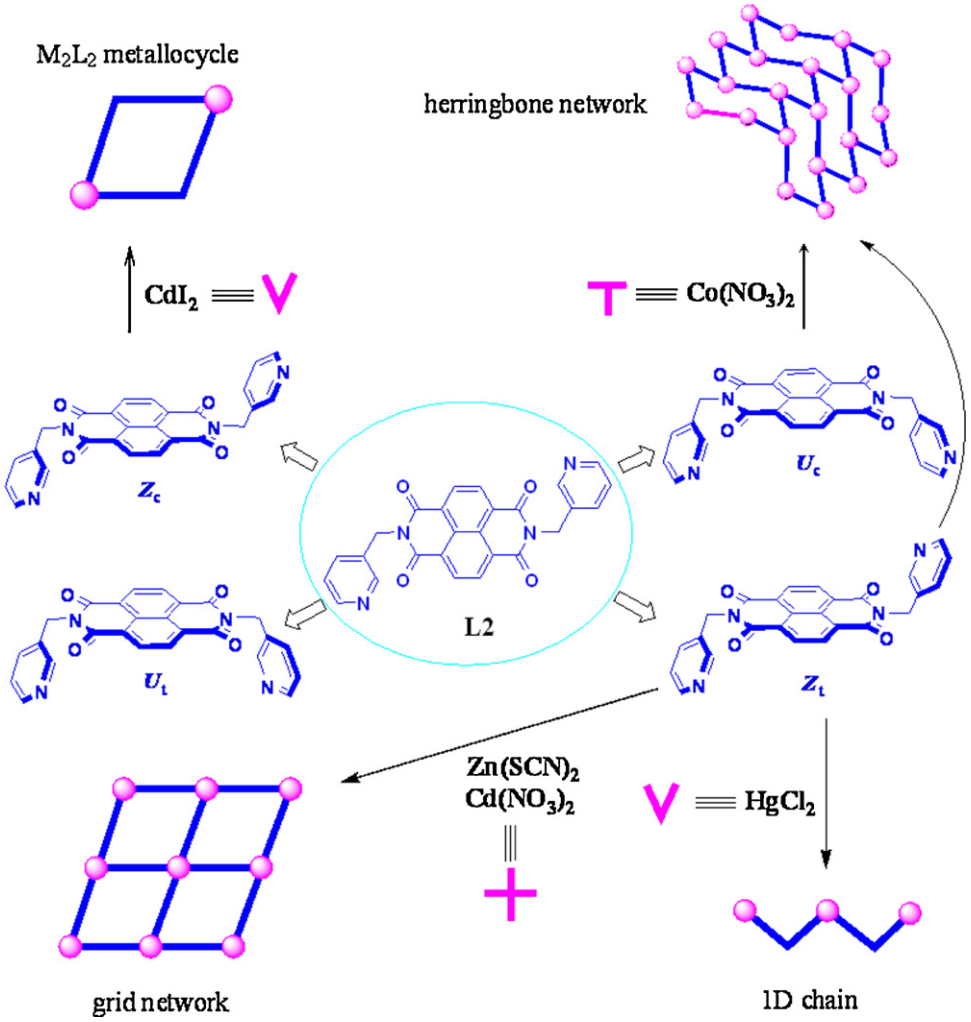

Fig. 3. Possible conformational modes of ligand **L2** and formation of different coordination assemblies. (*Z* for *anti* orientation of the Py rings and *U* for *syn* orientation of the Py rings, t for transoid orientation of the Py rings and c for cisoid orientation of the Py rings) [47].

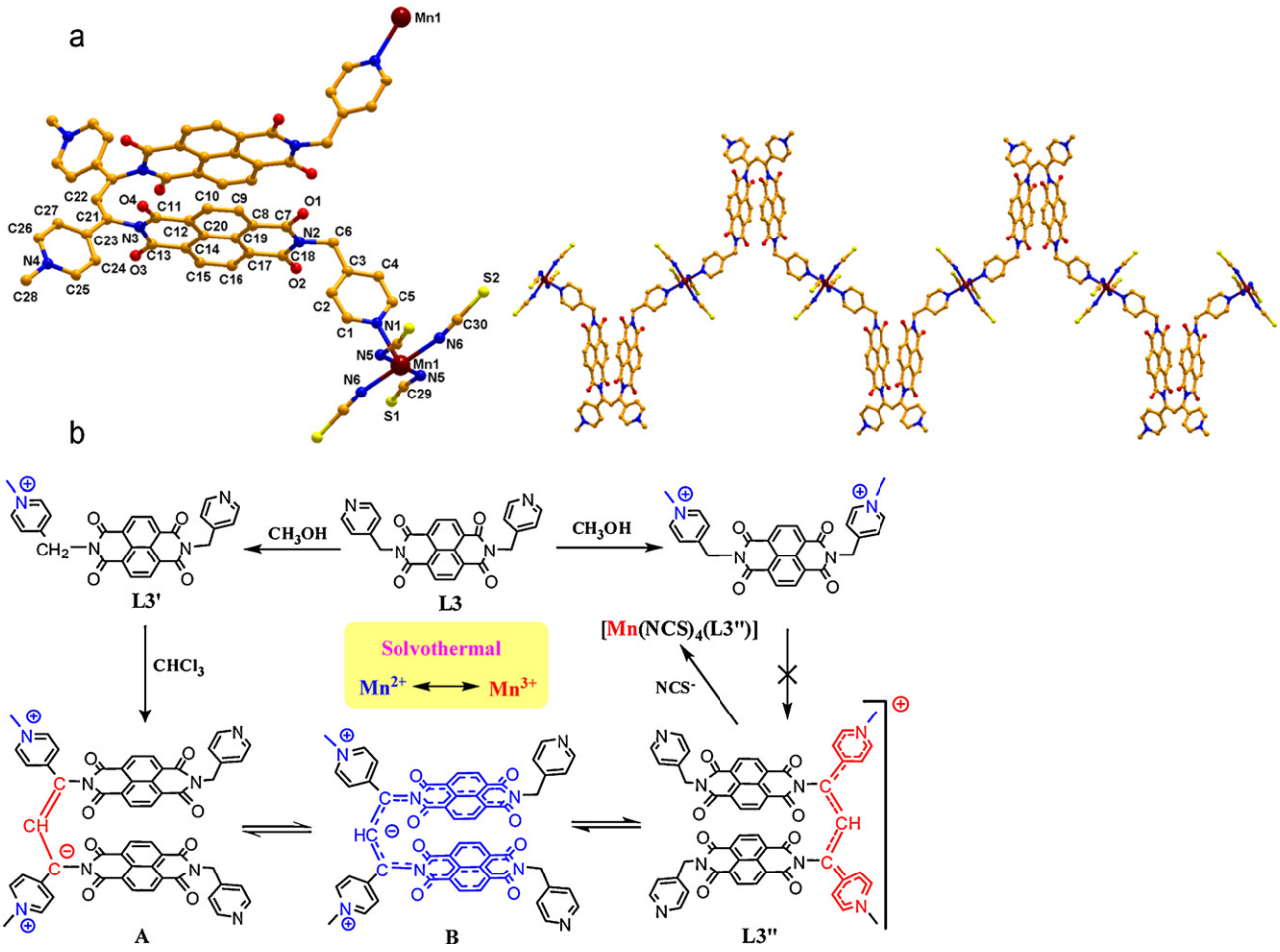

Fig. 4. (a) Crystal structures of the $[Mn(NCS)_4(\mathbf{L3}'')]$ motif (left) and the 1D chain in complex $\{[Mn(NCS)_4(L3'')]\cdot 2.5H_2O\}_n$ (right), (b) Possible procedures for the formation of compounds **L3**′ and **L3**″ and complex $[Mn(NSC)_4(\mathbf{L3}'')]$ from **L3** by solvothermal in situ metal/ligand reactions [48].

3. Structures of metal–organic materials assembled from different types of NDI

3.1. Structures based on pyridyl-terminated NDIs

Pyridyl termini are good candidates for the preparation of multifunctional ligands, and they can be connected to the diimide nitrogen sites of NDIs directly or through various linking groups like aryl, alkyl, alkylamino or ethyleneoxy to afford either rigid or flexible ligands. The rigid substituting termini will take on fixed conformations together with the NDI core components to enhance the structural robustness of the assembled coordination assemblies, while introduction of flexibility to the ligand termini to result in diversified coordination structures, subjected to multiplicate influences during assembling process.

Rigid ligand **L1** (*N*,*N*-di-(4-pyridyl)-1,4,5,8-naphthalenetetracarboxydiimide) was prepared with two 4-pyridyl termini directly connected to the central NDI core. It was applied to assemble a pillared metal–organic framework $Zn_2(NDC)_2(\mathbf{L1})$ (**L1**-Zn, NDC = 2,6-naphthalene dicarboxylate, Fig. 2). The crystal structure comprises square grids with paddle-wheeled $[Zn_2(COO^-)_4]$ sub-units acting as 6-connecting nodes. The sub-units are further connected by **L1** pillars to result in 3D microporous framework. Complex **L1**-Zn features in 2-fold interpenetration, yet retains 54% solvent-accessible void volume and shows robust and permanent porosity [45,46].

Semi-rigid ligand **L2** (*N*,*N*′-bis(3-pyridylmethyl)naphthalenediimide) has a rotatable $-CH_2-$ linker between the NDI core and pyridyl termini. Therefore, the ligand can adopt different conformations to produce various transition metal complexes with structures ranging from discrete 0D to polymeric 2D networks (Fig. 3) [47]. The large conjugate planes on the NDIs provide π–π interactions as well as hydrogen bonds to stabilize the crystal lattice. Photoluminescence was observed for the ligand and complexes.

Interestingly, similar semi-rigid ligand **L3** (*N*,*N*′-bis(4-pyridylmethyl) naphthalenediimide) brought, under solvothermal conditions, a series of rare in situ metal/ligand reactions during the assembly of a manganese coordination polymer. The single crystal structural analyses revealed an infinite 1D zigzag chain $\{[Mn(NPCS)_4(\mathbf{L3}'')]\cdot 2.5H_2O\}_n$ (Fig. 4a), in which a new ligand **L3**″ containing two conjugate NDI molecules was generated [48]. Spectroscopic study together with solid-state structures suggested the following reaction route: the original ligand **L3** was mono-*N*-methylated to give molecule **L3**″, and then two **L3**″ molecules were joined by double C–C coupling on $CHCl_3$ with full cleavage of the C–Cl bonds to afford **L3**″ (Fig. 4b).

By using ethyl-connected flexible pyridyl-terminated NDI ligand **L4**, discrete stable coordination complexes of Zn(II) porphyrins were formed, in which the metal center occupies a distal position (time averaged) through axial ligation as depicted in Fig. 5 [49].

Gao and coworkers prepared a threading intercalator, 0D complex **L5**-Ru shown in Fig. 6a, from reaction of *N*,*N*̃-bis[(3-propyl)-imidazole]-1,4,5,8-naphthalene diimide imidazole (**L5**) and $Ru(bpy)_2Cl$ (bpy = 2,2̃-bipyridine). This complex selectively interacts with double stranded (*ds*-) DNA with great stability and

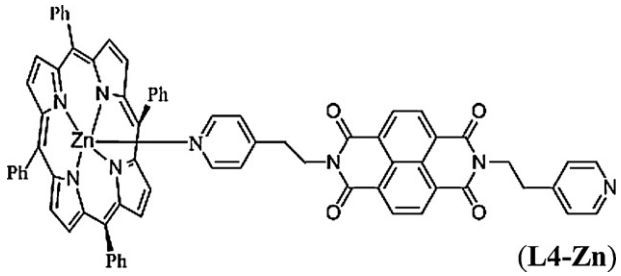

Fig. 5. Simple dyad ensembles utilizing Zn–N coordination bond [49].

was further immobilized on the surface of an electrochemical DNA biosensor and used in DNA quantification [50].

For alkylamino-mediated flexible ligand **L6**, a 2 + 2 type ring structure was generated by the confirmation of ESI-MS data. The free rotating methyl-pyridine groups at the termini of NDI were considered to capture Zn(II) ions firstly to form **L6**-Zn. When pyrophosphates (PPi) were added, Zn(II) ions further coordinate with the oxygen atoms on PPis to give a tetranuclear circular complex (Fig. 6b). The π–π interactions are formed between the large naphthalene planes, leading to strong fluorescence originated from excimer formation [51].

3.2. Structures based on bipyridyl-terminated or terpyridyl-bridged NDIs

Attaching one bipyridyl (bpy) terminus to NDI affords an unsymmetrical ligand **L7.** This ligand was coordinated with Ru(II) and further linked to amino acid group such as tyrosine to form donor–photosensitizer–acceptor (D–P–A) triad assemblies (**T1–T3**, Fig. 7). Long-lived charge-separated states in the ns to ms range were observed upon laser flash excitation in these systems. Tris(bipyridine)ruthenium(II) serves as photosensitizer, naphthalene diimide as acceptor, and hydrogen bonded phenol as donor [52,53].

Construction of dynamic molecular tweezers was achieved by metal-ion coordination with a terpyridyl-bridged ligand **L8** or analogous ligands **L9** and **L10** (Fig. 8). The presence of large aromatic naphthalene diimide moieties on the scaffold of the molecular tweezers brought additional supramolecular interactions and significantly influenced the self-assembly process [54].

3.3. Structures from carboxylic-, sulfonic-, phosphonic- or phosphanyl-terminated NDIs

A new class of inclusion complex (**L11**-Ni) composed of encapsulating metallocavitands and naphthalene diimide units was prepared from carboxylic-terminated NDI ligand **L11**, in which the naphthalene diimide was included between the two metallocavitand hemispheres (Fig. 9). The complexes were readily prepared and existed as stable and discrete complexes in both solution and solid state, and exhibited rich redox chemistry. The complexation of **L11** by Ni_2L' (L′ = 24-membered Robson-type hexaaza-dithiophenolate ligand) fragments results in a negative potential shift of the diimide centered redox process, and the two dinuclear nickel(II) subunits behave as two independent redox-groups owing to the large distance of ca. 19 Å between them [55].

A sulfonic-terminated NDI ligand **L12,** *N*,*N*′-Bis(4-phenylsulfonate)-1,4,5,8-naphthalene tetracarboxyl diimide, was prepared as the disodium or bis(tetrabuty1ammonium) salts. These salts could be reduced either electrochemically in DMF or water or by dithionite in water to form an anion radical. Spectroscopic study revealed that such an anion radical can form a monomer in DMF, dimer in water, or aggregate in aqueous NaCl to form π-stacks that are spectroscopically similar to the stacks formed in a solid film of the same radical [56].

From phosphonic-terminated NDI ligand **L13**, a new Ni(II) layered organic/inorganic hybrid compound was prepared in very mild conditions. The X-ray powder structure characterization suggested a pillared-layer organic/inorganic hybrid structure. The inorganic layers consist of corner sharing $[NiO_5(H_2O)]$ octahedra which are pillared by the phosphonic-terminated NDI ligand **L13**, as depicted in Fig. 10. The distance between the organic and inorganic layers is 17.8 Å [57].

In another case, Politi and co-workers constructed photoactive thin films from the same phosphonic-terminated NDI ligand

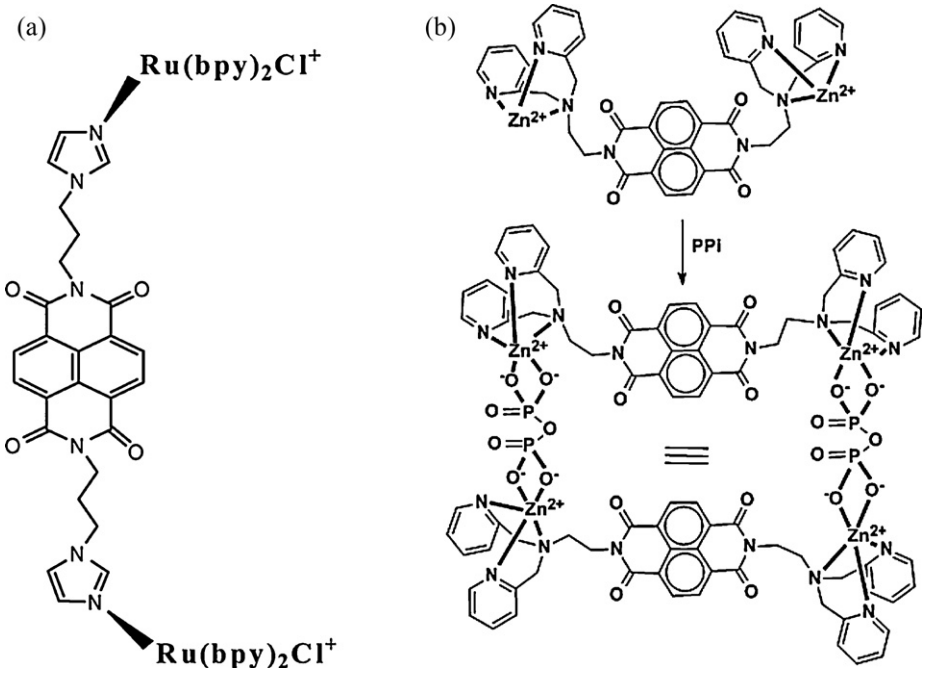

Fig. 6. (a) A threading intercalator from NDI and $Ru(bpy)_2Cl$ [47], (b) A 2 + 2 ring yielded from binding of pyrophosphate (PPi) with **L6**-Zn [51].

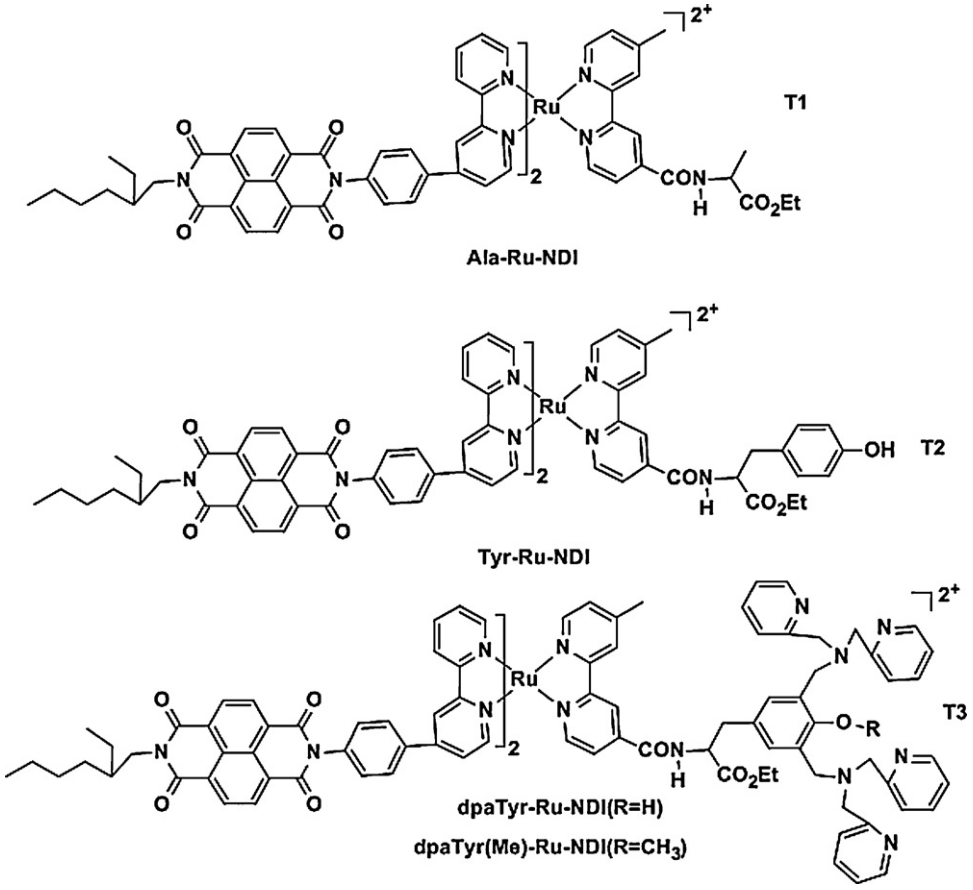

Fig. 7. Structures of D–P–A assemblies based on bpy-ended NDIs [52,53].

L13 with zirconium phosphonate upon silica or quartz substrates (Fig. 11). NDIs stack efficiently within the layers, and strong excimer-like emission can be observed from fluorescence measurements (λ_{ex} = 355 nm) [28]. They also fabricated a nanohybrid xerogel from the condensation of tetraethyl orthosilicate (TEOS) in the presence of **L13**. Physical and chemical characterization of the materials revealed that the morphology of the hybrid xerogels is quite different from that of xerogels without **L13** and the materials show efficient photo-oxidation effects [58]. Similar kinds of hybrid materials were further studied for bio-molecular purposes [59].

Naphthalene diimide moieties were also incorporated into a hemilabile phosphanyl-alkyl thioether ligand to give ligand **L14**. Reaction of this ligand with Cu(II) and Rh(II) formed condensed intermediates via a weak-link approach as shown in Fig. 12. In such intermediates, the two diimide units were cofacially aligned within a supramolecular macrocyclic architecture. However, introduction of ancillary ligands to such condensed intermediates will cause the weak thioether-metal bonds to break, thus generating a large macrocycle in which the distance between diimide units is significantly larger than in the condensed intermediates (Fig. 12) [60].

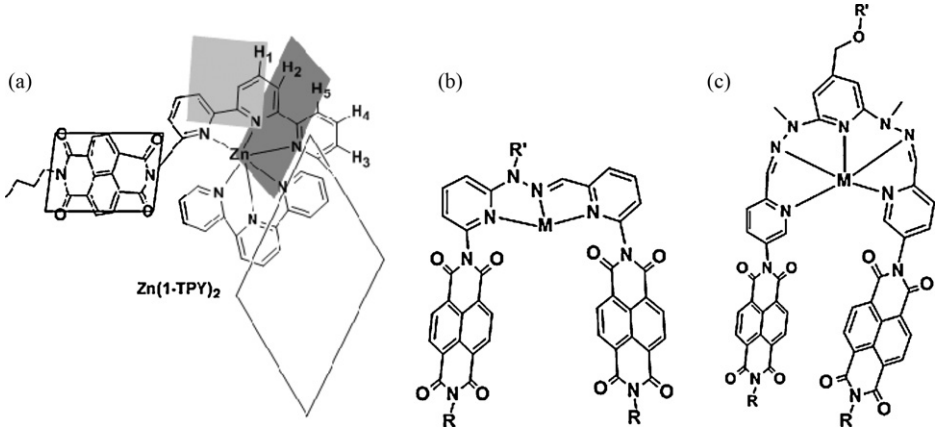

Fig. 8. Structures of the metallo-controlled molecular tweezers from terpyridyl-bridged NDI ligand **L8** (a) or its analogous ligands **L9** (b) and **L10** (c) [54].

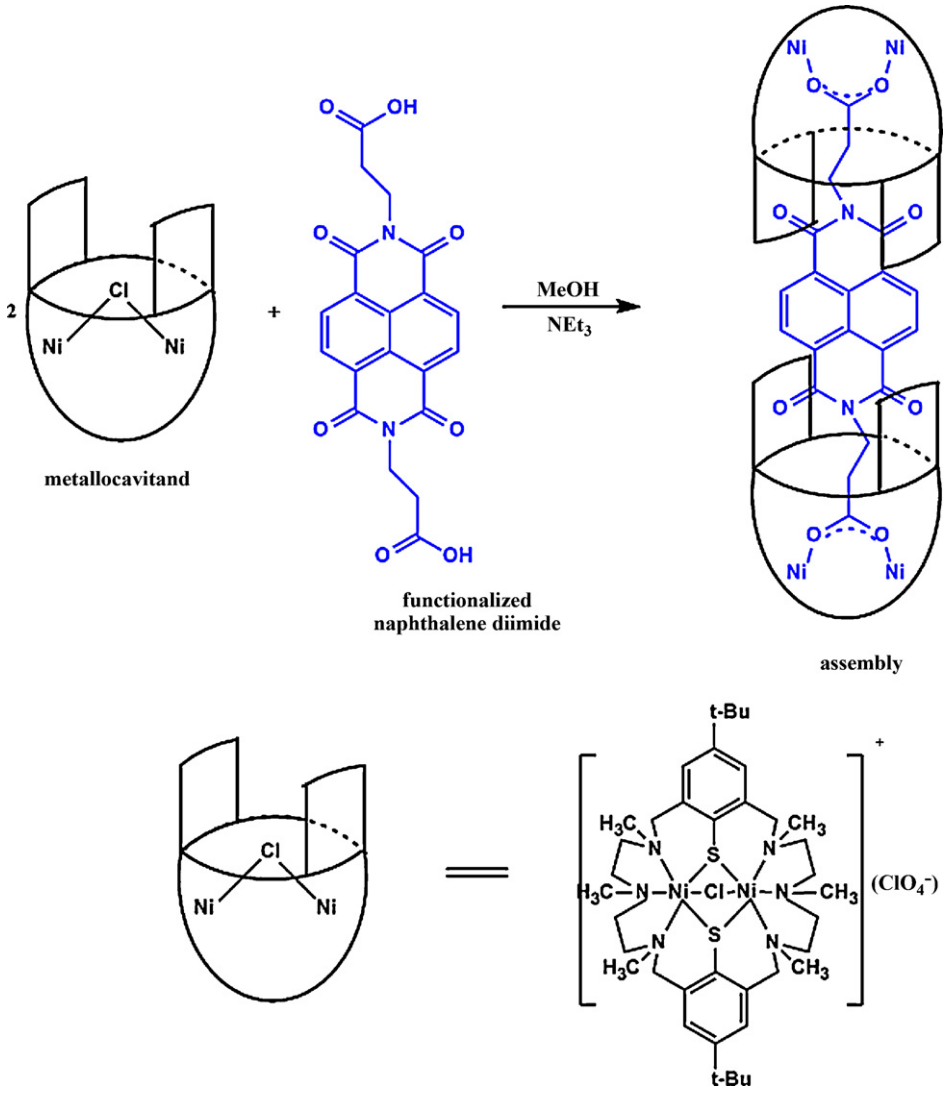

Fig. 9. Schematic representation of the encapsulation of the di-functionalised naphthalene diimide **L11** by a binucleating metallocavitand to yield the inclusion complex [55].

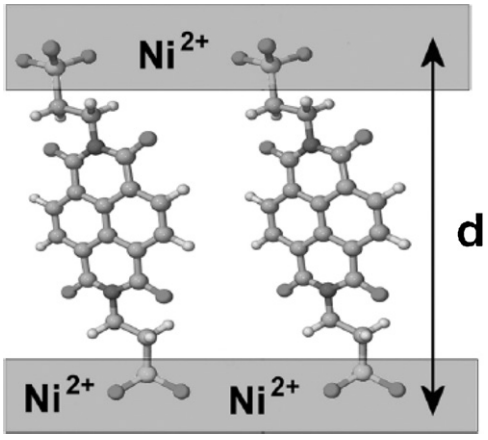

Fig. 10. Schematic structural model for the layered organic/inorganic hybrid compound formed by phosphonic-ended NDI ligand **L13**.
Reprinted with permission from Ref. [57]. Copyright 2008 Elsevier.

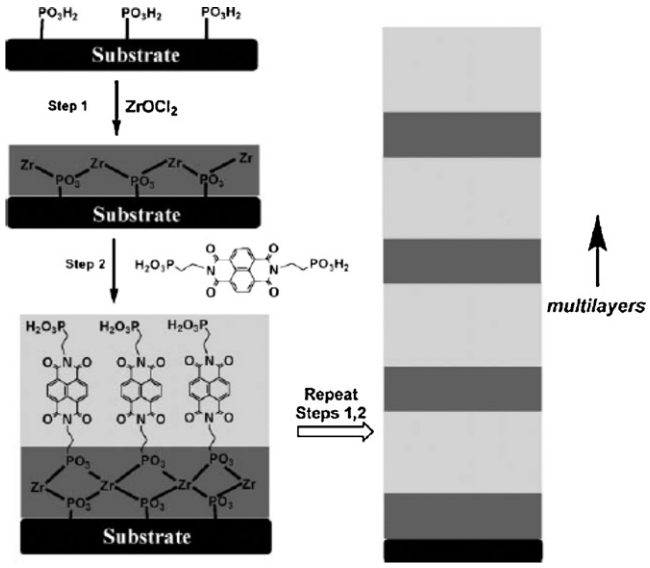

Fig. 11. Controlled growth of **L13**-Zr thin films on silica electrodes leads to multilayers.
Reprinted with permission from Ref. [31]. Copyright 2008 RSC.

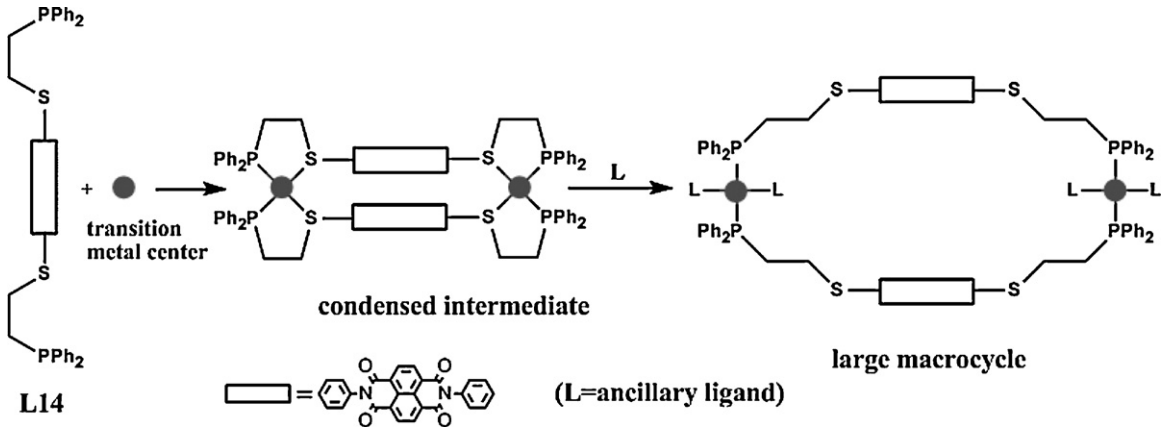

Fig. 12. Condensed intermediate and large macrocycle formed from phosphanyl-ended ligand **L14** [60].

3.4. Structures based on acetylene-terminated NDIs

Acetylene-terminated NDIs ligands have been extensively studied in assembly of Pt(II) organometallic complexes which comprise an electron donor–photosensitizer–acceptor (D–P–A) triad motif. The triad can undergo photoinduced charge separation (PCS) to produce the PCS state D^+-Pt-A^-, similar to the case in the Ru(II) complex described in section 3.2. In the triads MTA-Pt-MNDI (**T4**) and MTA-Pt-NDI (**T4′**) shown in Fig. 13a, dimethoxydimethyltriphenylamine (MTA) serves as the electron donor and a naphthalene diimide [(M)NDI] as the acceptor. These chromophores were bonded to the Pt moiety through highly twisted phenylene ethynylene linkages [61]. The research was further extended using a series of platinum acetylides of varying lengths as the linking spacer, (diphenylamino)-2,7-fluorenylene (DPAF) unit as the donor and NDI as the acceptor (**T5–T7**, Fig. 13b). Analyses of the experimental results led to a model in which charge separation and charge recombination occurred by hole hopping via states localized on the $[-Pt(PBu_3)_2-C{\equiv}C-Ph-C{\equiv}C-]_n$ bridge [62].

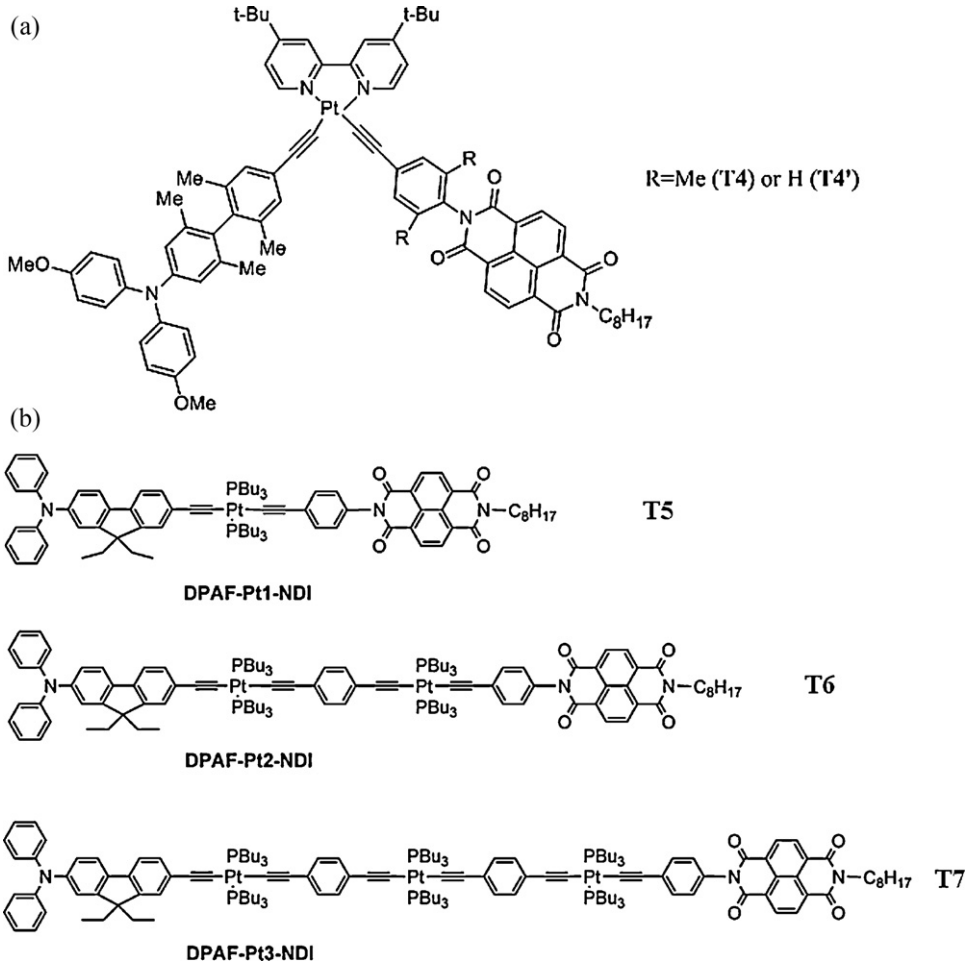

Fig. 13. Molecular structures of D-Pt-A type complexes based on acetylene-ended NDIs ligands [61,62].

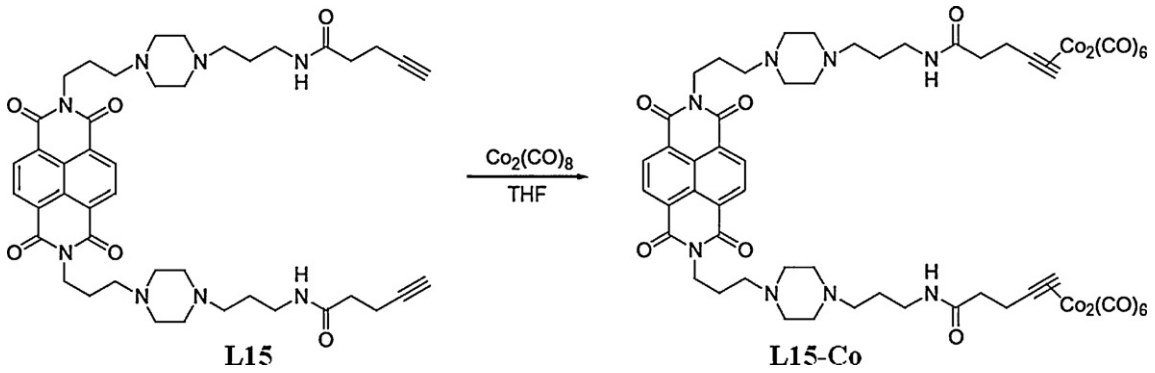

Fig. 14. DNA binding compounds based on ligand **L15** [63].

An NDI ligand having two long and pliable arms with acetylene-terminated groups (**L15**) reacts with dicobalt hexacarbonyls at its substituent termini to give complex **L15-Co** (Fig. 14). Comparison of the binding ability of **L15-Co** and **L15** with double stranded (*ds*-) DNA by means of threading intercalation mode disclosed that the bulky substituent in the metal complex **L15-Co** could act as anchor to prevent dissociation of intercalator from DNA [63].

3.5. Other structures based on covalently functionalized NDIs

In 1993, Osuka and coworkers synthesized a series of fixed-distance triads (labeled as **T8** a–d) consisting of zinc porphyrin (ZnP), free-base porphyrin (H_2P) and naphthalene diimide moieties which are bridged by aromatic spacers. As seen from Fig. 15a, the center-to-center distance between ZnP and H_2P can be modulated by the length of the spacers from 13 to 17.2 Å. The lifetimes and efficiency of the charge-separated states across the series exhibited distance dependent behavior [34].

Triad **T9** (Fig. 15b) bearing a Zn(II) porphyrin donor with pyromellitimide (PMI) and NDI acceptors was further synthesized. By modulating the electronic coupling between donor and acceptors, the direction of intramolecular electron transfer can be controlled [35].

NDIs containing covalently bonded functional groups have also been widely used in assembly of organic supramolecules as the components for rotaxanes or catenanes. For example, the donor–acceptor pair of electron-deficient NDI and electron-rich DN38C10 crown ether were incorporated into three different types

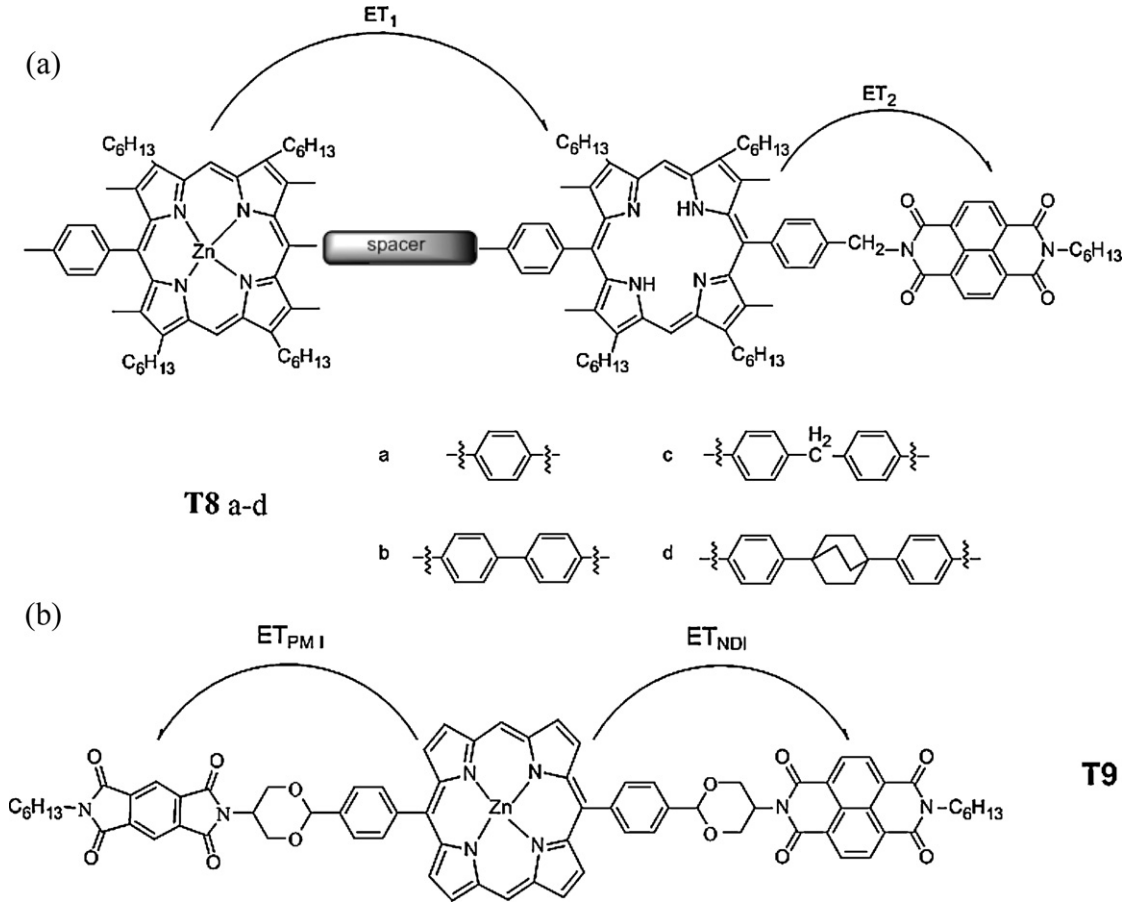

Fig. 15. Examples of artificial porphyrin triads based on NDIs. (a) Osuka's system **T8** a–d, [31], (b) Triad **T9** which bears two acceptors was used to demonstrate ET (electron transfer) switching between NDI and PMI groups [35].

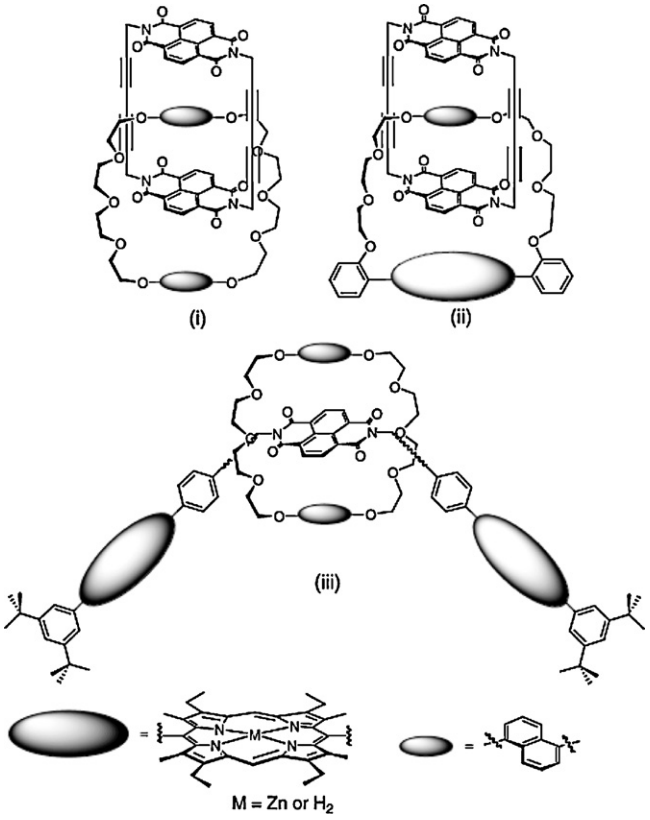

Fig. 16. Rotaxanes or catenanes based on NDIs.
Reprinted with permission from Ref. [64]. Copyright 2008 Taylor&Francis.

of rotaxanes or catenanes, as illustrated in Fig. 16: (i) organic catenanes with propynyl naphthalene diimide as a component, (ii) metallo-porphyrin extended catenanes of similar structure and (iii) [2]rotaxanes incorporating NDI as the central recognition unit of the linear components of the rotaxane, and a crown ether encircling it with two free-base porphyrin groups as stoppers. The fundamental design principles rely on charge-transfer (CT) interaction between the π-donor and π-acceptor complementary components [64].

4. Analytical techniques used in study of the NDIs systems

4.1. Cyclic voltammetry (CV)

As mentioned above, NDIs tend to undergo reversible one-electron reduction to form stable radical anions. Cyclic voltammetry is a straightforward method to track this electron-transfer process. For example, in a Pt-bpy*-cat-NDI (bpy* = 4,4ĭ-di-tert-butyl-2,2ĭ- bipyridine, cat = catechol) triad system (**T10**, Fig. 17a), cyclic voltammetry showed three partially overlapping reduction processes (Fig. 17b). The first and the second one-electron reductions, at −1.03 and −1.48 V vs. ferrocenium/ferrocene (Fc^+/Fc), respectively, were located on the 1,4,5,8-naphthalenediimide group, while the third reduction at −1.85 V was centered on the bpy* ligand. In addition, there was one reversible oxidation process occurred at +0.07 V, which was centered on the catecholate moiety [65].

Different zinc porphyrin-naphthalenediimide dyads and zinc porphyrin-pyromellitic diimide-naphthalenediimide triad have been prepared to examine the effects of metal ions on photoinduced charge-separation (PCS) and charge-recombination (CR) processes. Scandium triflate $Sc(OTf)_3$ or lutetium triflate $Lu(OTf)_3$ were used

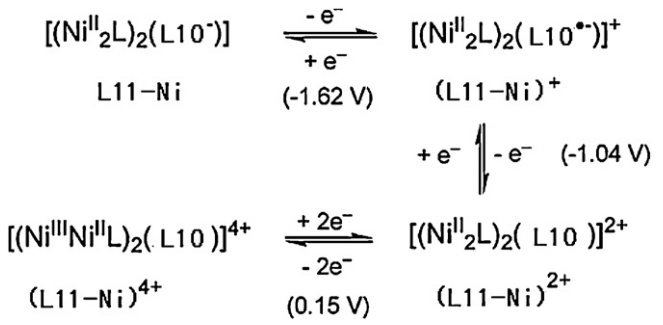

Scheme 2. Assignment of redox processes for a ternary complex (L11-Ni) composed of NDIs and binucleating metallocavitands.
Reprinted with permission from Ref. [55]. Copyright 2009 RSC.

and both can bind with the NDI radical anion. Taking the dyad system ZnP-NDI as an example, cyclic voltammetry analyses found that one electron reduction potential (E_{red}) of the NDI moiety was shifted in a positive direction with increasing metal ion concentration, whereas the one-electron oxidation potential of the ZnP moiety remains the same (Fig. 18). The neutral species of NDI cannot bind with metal ions, so the driving force of the PCS process is the same as that in the absence of metal ions. Whereas due to the strong binding of the metal ion with NDI^-, the driving force of the CR process decreases with increasing metal ion concentration. Therefore, this study provides a new strategy for controlling the back electron-transfer processes of the charge-separated states by complexation with metal ions [66].

In non-D–P–A type system **L11**-Ni containing NDI and binucleating metallocavitands described in Section 3.3, cyclic voltammetry showed three redox waves at −1.62, −1.04 and 0.15 V vs. ferrocenium/ferrocene (Fc^+/Fc), respectively. The processes at −1.04 and −1.62 V corresponded to the reduction of the dication (**L11**-Ni)$^{2+}$ to (**L11**-Ni)$^+$ (bearing the radical anion $NDI^{\bullet-}$) and the reduction of (**L11**-Ni)$^+$ to neutral **L11**-Ni (bearing the doubly reduced NDI ligand), respectively. The redox wave located at 0.15 V on the other hand was tentatively assigned to a two-electron metal centered $Ni^{II}Ni^{II} \rightarrow Ni^{II}Ni^{III}$ oxidation yielding the mixed-valent tetrametallic tetracation. These redox-processes are summarized in Scheme 2 [55].

4.2. UV–vis absorption spectroscopy and spectroelectrochemistry

The UV–vis absorption bands at low energies (360–380 nm) are typical for naphthalene diimides and even lower peaks (>400 nm) will be observed when they are reduced to anion radicals. Therefore, UV–vis could be applied to identify the existence and states of NDIs in a complex system [44].

The combination of electrochemistry and UV–vis spectrometry (UV–vis spectroelectrochemistry) can allow one to determine the nature of the frontier orbitals, the chemical reversibility of the redox processes, and the electrochromic properties of NDI-containing complexes. For example, in the triad system Pt-bpy*-cat-NDI (**T10**, Fig. 17a), changes in the absorption spectra in the course of one-electron oxidation revealed that the oxidation was accompanied by a depletion of the LLCT absorption band (506 nm at 253 K), and the formation of several new bands in the visible spectroscopic region with maxima in the range of 456–470 and 580–621 nm (Fig. 19a). These bands can be assigned to absorption of a semiquinone radical cation coordinating to Pt(II). Furthermore, the curves disclosed that at early times during the electrolysis, a band at ca. 650 nm appeared and then diminished as electrolysis progressed. The above behavior can be attributed to generation of intermediate species during oxidation. The reduction of the complex was accompanied by the disappearance of

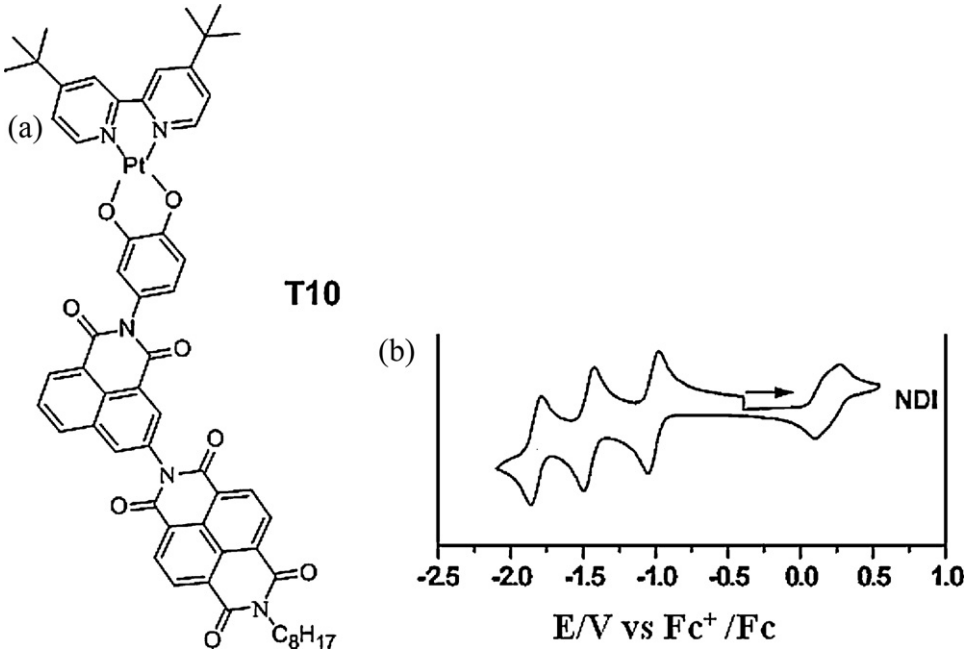

Fig. 17. Triad system Pt-bpy*-cat-NDI **T10** (a) and its cyclic voltammogram vs. ferrocenium/ferrocene (Fc^+/Fc) (b).
Reprinted with permission from Ref. [65]. Copyright 2008 ACS.

the absorption bands of 1,8-naphthalimide chromophore at 350 and 334 nm, and the concomitant formation of the new absorption bands with maxima at 815, 739, 492, 422, and 273 nm, characteristic for the 1,8-naphthalimide anion radical (Fig. 19b) [65].

Transient absorption measurements are very useful in detecting the intermediates which are generated during the electron transfer process. For example, one can observe the different PCS states and follow the dynamics of their formation and decay. In a series of triad systems with Zn(II) porphyrin (ZnP) compounds covalently linked to different naphthaleneimide (NI) and naphthalenediimide (NDI) electron acceptor units (**T11**, Fig. 20), transient absorption measurements demonstrated a selective direction of electron transfer under different conditions. Excitation to the lowest excited S1 state of the porphyrin (Q-band excitation) would give electron transfer

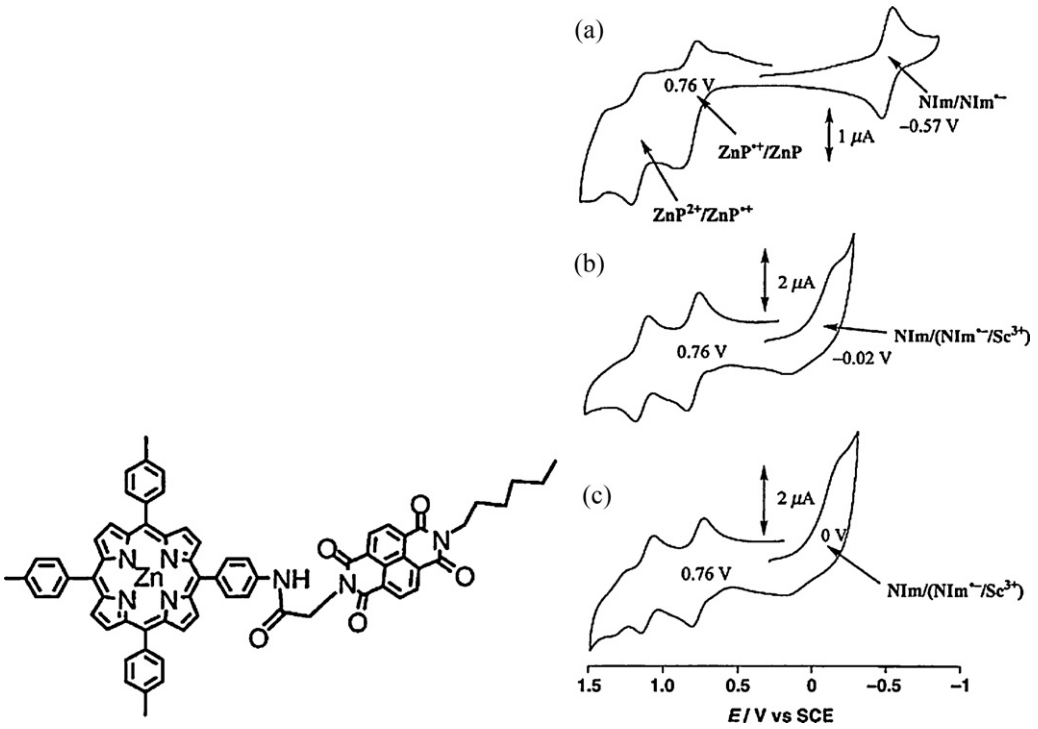

Fig. 18. Dyad system ZnP-NDI (left) and cyclic voltammograms (right, 5.0×10^{-4} M): (a) in the absence of Sc^{3+}, (b) in the presence of 3.0×10^{-3} M Sc^{3+}, and (c) in the presence of 5.0×10^{-3} M Sc^{3+} in deaerated PhCN solution containing $TBAPF_6$ (0.10 M) at 298 K vs. the saturated calomel electrode (SCE).
Reprinted with permission from Ref. [66]. Copyright 2004 Wiley-VCH.

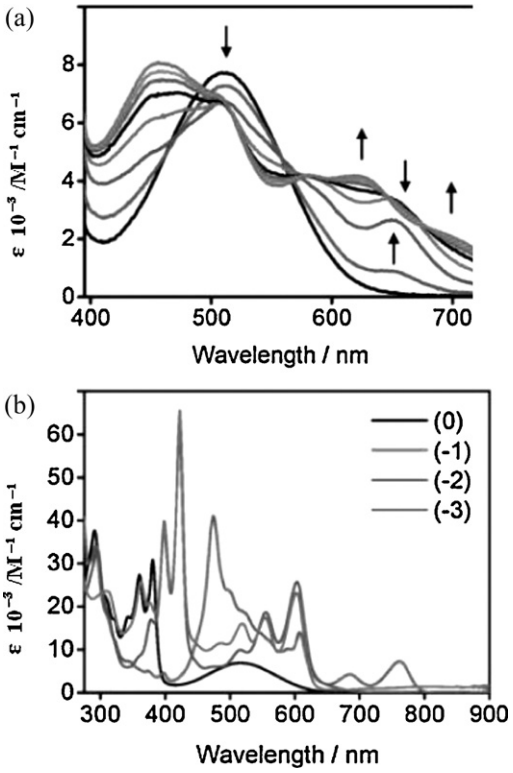

Fig. 19. (a) Changes in the absorption spectra in the course of one-electron oxidation of 0.5 mM Pt-bpy*-NDI in CH_2Cl_2 containing 0.4 M $[NBu_4][PF_6]$ at 253 K. (b) Absorption spectra of the neutral and one-/two-/three-electron reduced forms of the complex Pt-bpy*-NDI in DMF containing 0.2 M $[NBu_4][PF_6]$ at 253 K obtained from the spectroelectrochemical experiments performed on 0.5 mM solution. The first two reduction processes were centered on the 1,4,5,8-naphthalenediimide group, and the third reduction was centered on the bpy* ligand.
Reprinted with permission from Ref. [65]. Copyright 2008 ACS.

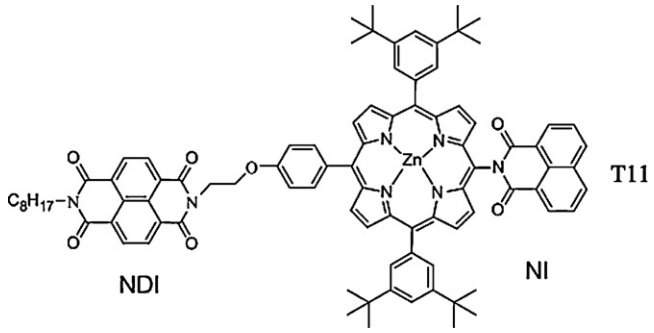

Fig. 20. Triad system **T11** [67].

to the NDI unit, while excitation to the higher S2 state (Soret-band excitation) would give electron transfer to the NI unit [67].

4.3. EPR spectroscopy

Because there are intermediate species in the oxidation process of NDI-containing compounds, and some would be EPR active ($S = ½$), EPR spectroscopy offers a chance to gain further insight into the electron transfer behavior into the nature of the frontier orbitals.

The photoinduced reactions in the $Mn_2^{II,II}$-Ru^{II} -NDI triad (**T12**, Fig. 21a) were studied at 140 K. Light-induced electron transfer reactions occur, and products, long-lived enough to be trapped for EPR analysis, are formed. After 50 flashes (Fig. 21b), the signal intensity of $Mn_2^{II,II}$ had decreased by 10% concomitantly with an increase of the $Mn_2^{II,III}$ signal. In addition, a narrow signal from a radical appeared in the $g = 2$ region, typical for the $NDI^{\bullet-}$ radical. Continued laser flashing of the sample resulted in a further decrease of $Mn_2^{II,II}$ and an increase of $Mn_2^{II,III}$, as well as an increase of the $NDI^{\bullet-}$ radical signal [68].

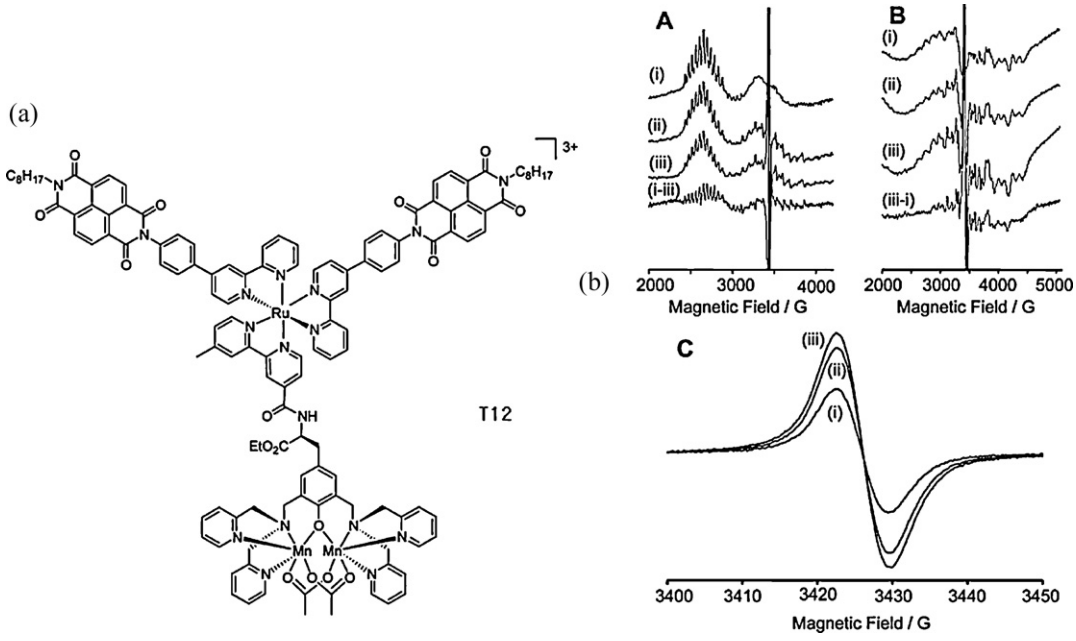

Fig. 21. $Mn_2^{II,II}$-Ru^{II} -NDI triad (a) and its EPR spectra (b): recorded at 11 K (panels A and C) or 4 K (panel B) in the (i) dark, after (ii) 50 flashes and (iii) 250 flashes given to the sample at 140 K. Spectrum (i–iii) in panel A is the difference spectrum showing the decrease of the $Mn_2^{II,II}$ after 250 flashes, and spectrum (iii–i) in panel B shows the corresponding increase in $Mn_2^{II,III}$. Each spectrum is the average of four scans. Panel C shows the EPR spectra of the $NDI^{\bullet-}$ radical recorded during the same 140 K flash photolysis experiment after (i) 50 flashes, (ii) 150 flashes, and (iii) 500 flashes.
Reprinted with permission from Ref. [68]. Copyright 2005 ACS.

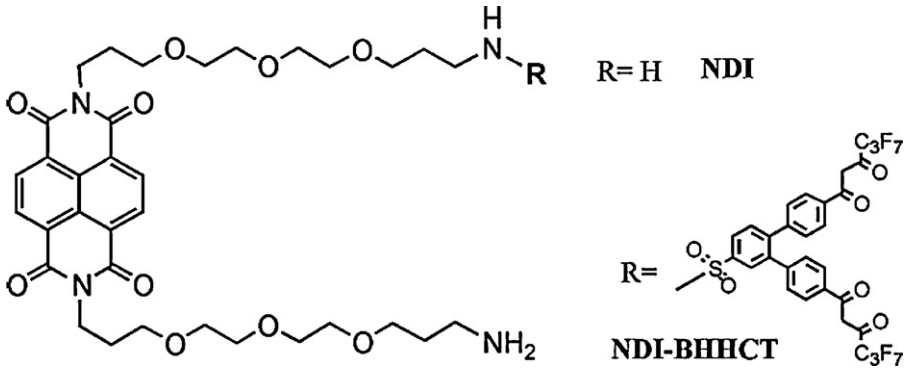

Fig. 22. Structures of the investigated (NDI–BHHCT) ligand and the reference compound (NDI) [69].

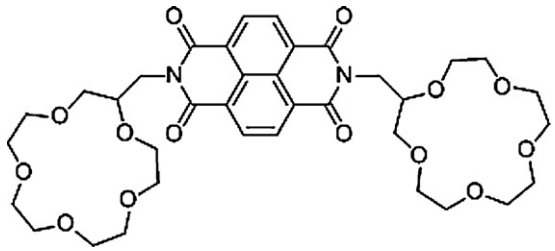

Fig. 23. NDI ligand bearing bis-crown pendants can serve as a prototype for the chemosensing of Ba^{2+} [70].

5. Potential applications

5.1. Artificial models for photo-induced electron transfer

NDIs were widely used in mimicking the natural photosynthetic process of converting light energy into chemical energy because of their electron accepting properties. Usually, in gaining efficient photo induced electron transfer, a D–P–A type system is preferable. Long-lived PCS states are produced by a sequence of vectorial electron transfer that takes the electron to an acceptor separated from the donor via a bridge. As mentioned before, a lot of porphyrin-connected triads, Pt(II)-organometallic systems, or Ru(II)-bpy-connected triad systems have been designed from different NDI ligands to achieve the PCS states.

In the porphyrin triads system **T8** mentioned in Section 3.5, upon photoexcitation (λ_{ex} = 532 nm), long-lived PCS states in the range of 0.14–80 μs were obtained by a relay approach in THF solvent. The steady-state fluorescence and transient absorption techniques indicated the occurrence of very efficient ($\phi \approx 0.8$) intramolecular singlet–singlet energy transfer from the zinc porphyrin to metal free porphyrin. Subsequently, charge transfer occurred between H_2P and NDI due to the formation of $(ZnP)^{\bullet+}$–H_2P–$(NDI)^{\bullet-}$ [34].

In simple supramolecular dyad **L4**-Zn formed from the axial ligation between NDIs and Zn(II) porphyrin described in Section 3.1, photoexcitation in non-polar solvents at 604 nm was evinced by transient absorption spectroscopy, and PCS states resulted with lifetimes of 1–100 μs depending on the solvent used [48].

Usually, metal (Ru, Ir, Pt) complexes that exhibit intense phosphorescence at room temperature via strong spin–orbit coupling (SOC) are desirable for generating efficient, long-lived PCS states. A highly efficient system (Φ_{PCS} = 0.96–0.97) with clear identification of the long lived PCS state was found in the triad system **T4** [60]. While in triads **T5–T7** (see Section 3.4), transient absorption spectroscopy on time scales ranging from 0.2 ps to 1 μs revealed that excitation of all of these complexes led to production of PCS states with nearly unit quantum efficiency [62].

Long-lived PCS states in the ns to ms range were observed in tris(bipyridine)ruthenium(II)-naphthalene diimide (NDI) triads **T1**–**T3** (see Section 3.2). For dpaTyr-Ru-NDI, the PCS yield was ~10%. The decay of the $NDI^{\bullet-}$ signal was biexponential with $k_b = 3.3 \times 10^6\ s^{-1}$ and $1.0 \times 10^5\ s^{-1}$, both with equal amplitudes. A third fraction, ~30% of the $NDI^{\bullet-}$ signal, was very long-lived and was quenched by oxygen on the minute time scale [52,53].

Triad system **T12** in Section 4.3 was the first synthetically linked electron donor–sensitizer–acceptor triad in which a manganese complex played the role of the donor. By time-resolved optical and EPR spectroscopy, the authors found that the average lifetime of

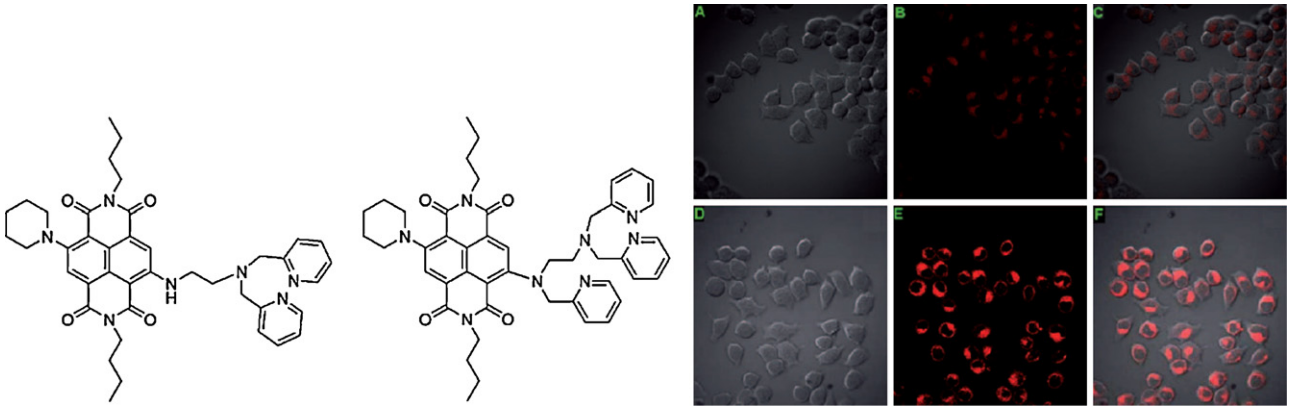

Fig. 24. (a) Two core-substituted NDIs ligands. (b) Confocal fluorescence images in KB cells: Top, (A–C) Cells incubated with PND (20 mm) for 0.5 h. Bottom, (D–F) Cells incubated with $ZnCl_2$ (20 mm) for 0.5 h then PND (20 mm) for 0.5 h. Emission was collected at 598–698 nm upon excitation at 543 nm. Bright field (A and D), fluorescence (B and E), and overlap field (C and F).
Reprinted with permission from Ref. [71]. Copyright 2010 Wiley-VCH.

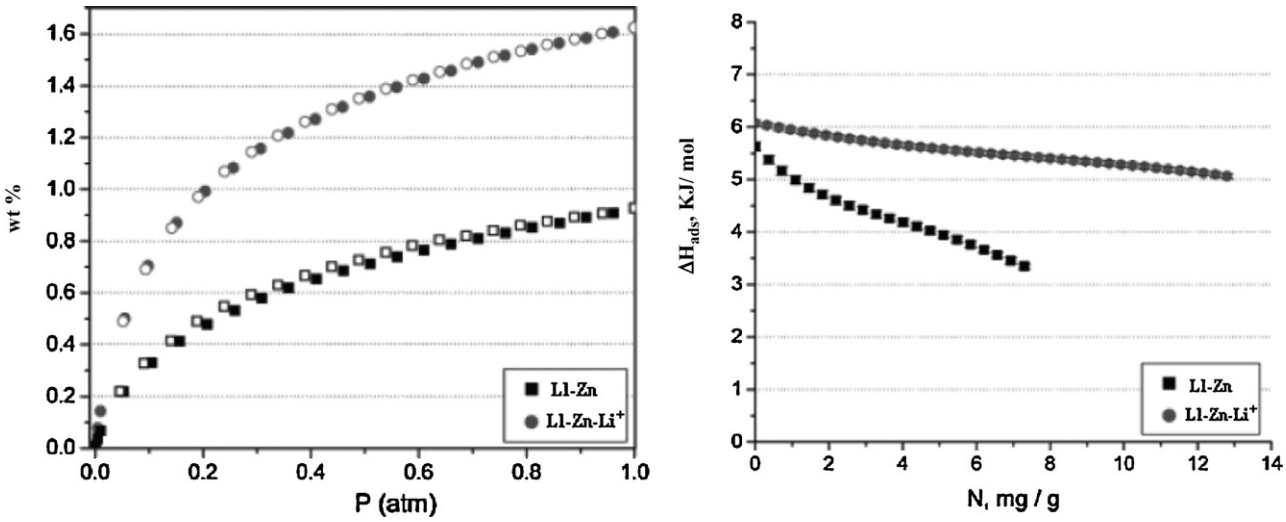

Fig. 25. H_2 adsorption isotherms at 77 K (a) and isosteric H_2 heat of adsorption (b) of **L1**-Zn and **L1**$^{-}$-Zn-Li^{+}.
Reprinted with permission from Ref. [46]. Copyright 2007 ACS.

the NDI$^{\bullet-}$ radical was ca. 600 μs at room temperature, at least 2 orders of magnitude longer than that for previously reported triads based on a $[Ru(bpy)_3]^{2+}$ photosensitizer. At 140 K, the intramolecular recombination was dramatically slowed, displaying a lifetime of 0.1–1 s. This was comparable to many of the naturally occurring PCS states in photosynthetic reaction center. The long recombination lifetime could be explained by an unusually large reorganization energy ($\lambda \approx 2.0$ eV) due to a large inner reorganization of the manganese complex [68].

As mentioned in Section 3.3, photoactive hybrid materials were prepared from NDI-based ligand **L13** with zirconium phosphonate on silica or quartz substrates (Fig. 11) [28,31]. This work was further extended by incorporating amino acids and peptides between the silica and zirconium/NDI phosphonate layers to form novel bioactive materials [30]. In another example, the increase of efficiency of tryptophan photooxidation was observed in the nanohybrid xerogel containing NDIs and was attributed to the presence of excitons due to NDI aggregates in the material. Therefore, an efficient approach was provided using this sol–gel method to prepare nanomaterials which can generate a stabilized transient species useful for the photooxidation of biomolecules [58].

5.2. Sensors

Complex **L5**-Ru in Section 3.1 shows a selective interaction with *ds*-DNA after immobilization on an electrochemical biosensor. Highly stable and reversible electrochemical oxidation/reduction processes were displayed in voltammetric tests and applied in DNA quantification. When the tests were carried out in an amine-containing medium, the signal-to-noise in amperometry was dramatically improved and as little as 3.0 attomoles of DNA can be detected in the sample solution. The increased sensitivity was attributed to the excellent catalytic activity of the redox moieties on **L5**-Ru towards oxidation of amines [50].

Complex **L15**-Co in Section 3.4 was further fabricated on a gold surface after hybridization with a complementary DNA strand. Using fourier transform infrared reflection absorption spectroscopy (FT-IR RAS) methods, absorption peaks assignable to the dicobalt hexacarbonyl complexes were obtained in the case of the formation of *ds*-DNA. This observation suggested that such an NDI-based complex can be used as an infrared probe for monitoring *ds*-DNA [63].

DNA detection can also be achieved by a rare earth complex of an NDI-based ligand. A naphthalenediimide derivative carrying a single bis(β-diketone)-*o*-terphenyl moiety (NDI–BHHCT) as shown in Fig. 22 was designed to chelate Eu^{3+} or Y^{3+} ions. The resulting complex was applied for the determination of calf thymus DNA. In the presence of DNA, the Eu^{3+} and Y^{3+} ternary complexes intercalated to DNA and resulted in proper arrangement on the DNA helix, thus enabling efficient energy transfer between the non-fluorescent Y^{3+} and fluorescent Eu^{3+} chelates. As a result, the enhancement of Eu^{3+} emission due to the co-fluorescence effect is observed in the presence of DNA. The calibration graph was linear up to 1.3 μg ml^{-1} with a detection limit of 12 ng ml^{-1} [69].

A pyrophosphate-selective fluorescent chemosensor was achieved at physiological pH in complex **L6**-Zn mentioned in Section 3.1, which can function in a 100% aqueous solution. The sensor showed an excimer peak at 490 nm only in the presence of PPi. Four zinc sites as well as a π–π interaction induced the unique 2 + 2 type excimer in the presence of PPi. Furthermore, the detection of PPi was selective over ATP (adenosine-triphosphate) or Pi (phosphate) [51].

On the other hand, a prototype for the chemosensing of Ba^{2+} based on self-assembling fluorescence enhancement was obtained by a novel bis-15-crown-5-naphthalene diimide derivative (Fig. 23). On the basis of the known ability of 15-crown-5 to interact with Ba^{2+}, a [2 + 2] adduct is formed, in which each Ba^{2+} ion coordinates to two 15-crown-5 subunits belonging to different molecules of the ligand. This [2 + 2] adduct favors the formation of an intramolecular excimer and displays a strong fluorescence enhancement to achieve the detection of Ba^{2+} [70].

Recently, Tian and coworkers reported two core-substituted NDI based ligands (Fig. 24a), which can serve as highly sensitive fluorescent probes for Zn^{2+}. Due to the differential binding mode of the connected substituents to different metals, the ligands show excellent selectivity to Zn^{2+} over other metal ions and are successfully used in imaging intracellular Zn^{2+} ions in the living KB cells (human nasopharyngeal epidermal carcinoma cell) (Fig. 24b) [71].

5.3. Gas adsorption

The framework of **L1**-Zn discussed in Section 3.1 afforded a good example of gas adsorption application by NDI-containing metal–organic materials. When the as-prepared framework was reduced by exposure to Li metal in DMF, the sample immediately changed color from bright yellow to brown, indicative of formation of **L1**$^{-}$-Zn-Li^{+}. The most astonishing feature of the reduced framework loading Li^{+} ions lies in that remarkable enhancements

were observed for H_2 sorption (Fig. 25a). At 77 K and 1 atm, the H_2 capacity of **L1**-Zn is 0.93 wt%, but for **L1**$^{-}$-Zn-Li^{+}, it is nearly double (1.63 wt%), and such is the case for the measured isosteric heat of adsorption (Fig. 25b). This phenomenon is quite notable because it represents a unique approach to enhance the sorption behavior of coordination frameworks by introducing unsaturated metal sites through chemical reduction [46].

Complexes and hybrid materials containing NDI ligands have also been studied for their potential applications in such fields as in situ reaction [48], magnetics [57], non-linear optics [72], and so on.

6. Conclusions

In general, as a type of versatile metal-containing material, the metal–organic coordination complexes and hybrid materials based on NDI ligands provide ideal models for the investigation of the relationships between molecular structures, reaction activities and their properties, especially in such procedures as photon–electron conversion and long-lived charge separation. The study and application of these models will promote novel molecular architectures, devices and machines that can bridge the gap between the molecular and macroscopic worlds.

Acknowledgements

This work was supported by the 973 Program of China (2007CB815302), the NSFC Projects (20821001, 20731005, 20903120, U0934003), the RFDP of Higher Education of China, and the Fundamental Research Funds for the Central Universities.

References

[1] J.J.I.V. Perry, J.A. Perman, M.J. Zaworotko, Chem. Soc. Rev. 38 (2009) 1400–1417.
[2] J.M. Lehn, Angew. Chem. 100 (1988) 91–116.
[3] Q. Zhang, J.Y. Zhang, Q.Y. Yu, M. Pan, C.Y. Su, Cryst. Growth Des. 10 (2010) 4076–4084.
[4] C. Janiak, Dalton Trans. (2003) 2781–2804.
[5] S.L. Qiu, G.S. Zhu, Coord. Chem. Rev. 253 (2009) 2891–2911.
[6] C.L. Chen, J.Y. Zhang, C.Y. Su, Eur. J. Inorg. Chem. 19 (2007) 2997–3010.
[7] W.H. Leung, Q.F. Zhang, X.Y. Yi, Coord. Chem. Rev. 251 (2007) 2266–2279.
[8] R.J. Kuppler, D.J. Timmons, Q.R. Fang, J.R. Li, T.A. Makal, M.D. Young, D.Q. Yuan, D. Zhao, W.J. Zhuang, H.C. Zhou, Coord. Chem. Rev. 253 (2009) 3042–3066.
[9] C.L. Chen, B.S. Kang, C.Y. Su, Aust. J. Chem. 59 (2006) 3–18.
[10] C. Janiak, J.K. Vieth, New J. Chem. 34 (2010) 2366–2388.
[11] U. Mueller, M. Schubert, F. Teich, H. Puetter, K. Schierle-Arndt, J. Pastre, J. Mater. Chem. 16 (2006) 626–636.
[12] Y.Y. Liu, Y.Q. Huang, W. Shi, P. Cheng, D.Z. Liao, S.P. Yan, Cryst. Growth Des. 7 (2007) 1483–1489.
[13] D.K. Cao, Y.Z. Li, Y. Song, L.M. Zheng, Inorg. Chem. 44 (2005) 3599–3604.
[14] Y.P. Cai, C.Y. Su, C.L. Chen, Y.M. Li, B.S. Kang, A.S.C. Chan, W. Kaim, Inorg. Chem. 42 (2003) 163–168.
[15] Y.H. Li, C.Y. Su, A.M. Goforth, K.D. Shimizu, K.D. Gray, M.D. Smith, H.C. zur Loye, Chem. Commun. (2003) 1630–1631.
[16] Z.M. Liu, Y. Liu, S.R. Zheng, Z.Q. Yu, M. Pan, C.Y. Su, Inorg. Chem. 46 (2007) 5814–5816.
[17] D.L. Reger, E.A. Foley, M.D. Smith, Inorg. Chem. Commun. 13 (2010) 568–572.
[18] L.D. Carlos, R.A.S. Ferreira, R.N. Pereira, J. Phys. Chem. B 108 (2004) 14924–14932.
[19] D.W. Dong, B.Z. Jiang, Mater. Chem. Phys. 78 (2003) 501–506.
[20] Q.M. Wang, B. Yan, Cryst. Growth Des. 5 (2005) 497–503.
[21] P. Mukhopadhyay, Y. Iwashita, M. Shirakawa, S. Kawano, N. Fujita, S. Shinkai, Angew. Chem. Int. Ed. 45 (2006) 1592–1595.
[22] W.W. Stewart, Nature 292 (1981) 17–21.
[23] M.R. Wasielewski, Chem. Rev. 92 (1992) 435–461.
[24] H. Shiratori, T. Ohno, K. Nozaki, I. Yamazaki, Y. Nishimura, A. Osuka, J. Org. Chem. 65 (2000) 8747–8757.
[25] D. Gosztola, M.P. Niemczyk, M.R. Wasielewski, J. Am. Chem. Soc. 120 (1998) 5118–5119.
[26] K.D. Johnstone, N. Bampos, J.K.M. Sanders, M.J. Gunter, New J. Chem. 30 (2006) 861–867.
[27] T. Iijima, S.A. Vignon, H.R. Tseng, T. Jarrosson, J.K.M. Sanders, F. Marchioni, M. Venturi, E. Apostoli, V. Balzani, J.F. Stoddart, Chem. Eur. J. 10 (2004) 6375–6392.
[28] M.A. Rodrigues, G.J.F. Demets, M.J. Politi, J. Mater. Chem. 12 (2002) 1250–1255.
[29] B.A. Jones, A. Facchetti, T.J. Marks, M.R. Wasielewski, Chem. Mater. 19 (2007) 2703–2705.
[30] H.E. Katz, A.J. Lovinger, C. Kloc, T. Siegrist, W. Li, Y.Y. Lin, A. Dodabalapur, Nature 404 (2000) 478–481.
[31] S.V. Bhosale, C.H. Jani, S.J. Langford, Chem. Soc. Rev. 37 (2008) 331–342.
[32] F. Würthner, S. Ahmed, C. Thalacker, T. Debaerdemaeker, Chem. Eur. J. 8 (2002) 4742–4750.
[33] J.L. Sessler, C.T. Brown, D. O'Connor, S.L. Springs, R. Wang, M. Sathiosatham, T. Hirose, J. Org. Chem. 63 (1998) 7370–7374.
[34] A. Osuka, R.P. Zhang, K. Maruyama, T. Ohno, K. Nozaki, Bull. Chem. Soc. Jpn. 66 (1993) 3773–3782.
[35] A. Osuka, R. Yoneshima, H. Shiratori, T. Okada, S. Taniguchi, N. Mataga, Chem. Commun. (1998) 1567–1568.
[36] U. Heinen, T. Berthold, G. Kothe, E. Stavitski, T. Galili, H. Levanon, G. Wiederrecht, M.R. Wasielewski, J. Phys. Chem. A 106 (2002) 1933–1937.
[37] C. Thalacker, C. Röger, F. Würthner, J. Org. Chem. 71 (2006) 8098–8105.
[38] S. Bhosale, A.L. Sission, P. Talukdar, A. Furstenberg, N. Banerji, E. Vauthey, G. Bollot, J. Mareda, C. Roger, F. Würthner, N. Sakai, S. Matile, Science 313 (2006) 84–86.
[39] H. Tanaka, S. Litvinchuk, D.H. Tran, G. Bollt, J. Mareda, N. Sakai, S. Matile, J. Am. Chem. Soc. 128 (2006) 16000–16001.
[40] V. Gorteau, G. Bollot, J. Mareda, A. Perez-Velasco, S. Matile, J. Am. Chem. Soc. 128 (2006) 14788–14789.
[41] C. Röger, M.G. Müller, M. Lysetska, Y. Miloslavina, A.R. Holzwarth, F. Würthner, J. Am. Chem. Soc. 128 (2006) 6542–6543.
[42] L.L. Miller, R.G. Duan, Y. Hong, I. Tabakovic, Chem. Mater. 7 (1995) 1552–1557.
[43] G. Andric, J.F. Boas, A.M. Bond, G.D. Fallon, K.P. Ghiggino, C.F. Hogan, J.A. Hutchison, M.A.P. Lee, S.J. Langford, J.R. Pilbrow, G.J. Troup, C.P. Woodward, Aust. J. Chem. 57 (2004) 1011–1019.
[44] S.J. Langford, M.J. Latter, C.P. Woodward, Photochem. Photobiol. 82 (2006) 1530–1540.
[45] B.Q. Ma, K.L. Mulfort, J.T. Hupp, Inorg. Chem. 44 (2005) 4912–4914.
[46] K.L. Mulfort, J.T. Hupp, J. Am. Chem. Soc. 129 (2007) 9604–9605.
[47] H.Y. Deng, J.R. He, M. Pan, L. Li, C.Y. Su, Cryst. Eng. Comm 11 (2009) 909–917.
[48] G.B. Li, J.M. Liu, Z.Q. Yu, W. Wang, C.Y. Su, Inorg. Chem. 48 (2009) 8659–8661.
[49] K.P. Ghiggino, J.A. Hutchison, S.J. Langford, M.J. Latter, M.A.P. Lee, M. Takezaki, Aust. J. Chem. 59 (2006) 179–185.
[50] Z. Gao, N. Tansil, Anal. Chim. Acta 636 (2009) 77–82.
[51] H.N. Lee, Z. Xu, S.K. Kim, K.M.K. Swamy, Y. Kim, S.J. Kim, J. Yoon, J. Am. Chem. Soc. 129 (2007) 3828–3829.
[52] O. Johansson, M. Borgström, R. Lomoth, M. Palmblad, J. Bergquist, L. Hammarström, L. Sun, B. Åkermark, Inorg. Chem. 42 (2003) 2908–2918.
[53] O. Johansson, H. Wolpher, M. Borgström, L. Hammarström, J. Bergquist, L.C. Sun, B. Åkermark, Chem. Commun. (2004) 194–195.
[54] S. Ulrich, A. Petitjean, J.M. Lehn, Eur. J. Inorg. Chem. (2010) 1913–1928.
[55] K.A. Lee, V. Lozan, S.J. Langford, B. Kersting, Dalton Trans. (2009) 7481–7485.
[56] J.F. Penneau, B.J. Stallman, P.H. Kasai, L.L. Miller, Chem. Mater. 3 (1991) 791–796.
[57] E.M. Bauer, C. Bellitto, C.J.G. Garcíab, G. Righini, J. Solid State Chem. 181 (2008) 1213–1219.
[58] M.A. Rodrigues, M.P. Bemquerer, N.D.S. Mohallem, M.J. Politi, Langmuir 22 (2006) 8939–8944.
[59] M.A. Rodrigues, M.P. Bemquerer, M.J. Politi, M.S. Baptista, J. Photochem. Photobiol. A 180 (2006) 218–221.
[60] M.S. Khoshbin, M.V. Ovchinnikov, K.S. Salaita, C.A. Mirkin, C.L. Stern, L.N.A.L. Zakharov, Chem. Asian J. 1 (2006) 686–692.
[61] S. Suzuki, R. Sugimura, M. Kozaki, K. Keyaki, K. Nozaki, N. Ikeda, K. Akiyama, K. Okada, J. Am. Chem. Soc. 131 (2009) 10374–10375.
[62] C. Liao, J.E. Yarnell, K.D. Glusac, K.S. Schanze, J. Phys. Chem. B 114 (2010) 14763–14771.
[63] K. Ohtsuka, K. Komizo, S. Takenaka, J. Organomet. Chem. 695 (2010) 1281–1286.
[64] M.J. Gunter, Z. Merican, Supramol. Chem. 17 (7) (2005) 521–528.
[65] N.M. Shavaleev, E.S. Davies, H. Adams, J. Best, J.A. Weinstein, Inorg. Chem. 47 (2008) 1532–1547.
[66] K. Okamoto, Y. Mori, H. Yamada, H. Imahori, S. Fukuzumi, Chem. Eur. J. 10 (2004) 474–483.
[67] S. Wallin, C. Monnereau, E. Blart, J.R. Gankou, F. Odobel, L. Hammarström, J. Phys. Chem. A 114 (2010) 1709–1721.
[68] M. Borgström, N. Shaikh, O. Johansson, M.F. Anderlund, S. Styring, B. Åkermark, A. Magnuson, L. Hammarström, J. Am. Chem. Soc. 127 (2005) 17504–17515.
[69] B. Juskowiak, I. Grzybowska, E. Galezowska, S. Takenak, Anal. Chim. Acta 512 (2004) 133–139.
[70] M. Licchelli, A.O. Biroli, A. Poggi, Org. Lett. 8 (2006) 915–918.
[71] X. Lu, W. Zhu, Y. Xie, X. Li, Y. Gao, F. Li, H. Tian, Chem. Eur. J. 160 (2010) 8355–8364.
[72] X.J. Liu, J.K. Feng, A.M. Ren, X. Zhou, J. Mol. Struct. (Theochem) 635 (2003) 191–202.